Applied Catalysis B: Environmental 91 (2009) 397–405

Contents lists available at ScienceDirect

Applied Catalysis B: Environmental

journal homepage: www.elsevier.com/locate/apcatb

One step activation of WO_x/TiO_2 nanocomposites with enhanced photocatalytic activity

Ahmed Khan Leghari Sajjad, Sajjad Shamaila, Baozhu Tian, Feng Chen, Jinlong Zhang *

Key Laboratory for Advanced Materials and Institute of Fine Chemicals, East China University of Science and Technology, 130 Meilong Road, Shanghai, 200237, PR China

ARTICLE INFO

Article history:
Received 28 April 2009
Received in revised form 8 June 2009
Accepted 9 June 2009
Available online 17 June 2009

Keywords:
WO_x/TiO_2 composite
Vacuum activation
Phenol degradation
Photocatalysis

ABSTRACT

New photocatalyst (WO_x–TiO_2) powder was successfully prepared by a sol–gel method with an attempt to extend light absorption of the TiO_2-based photocatalyst towards the visible light range and eliminate the rapid recombination of excited electrons/holes during photoreaction. The photo composite was characterized by X-ray diffraction (XRD), transmission electron microscopy (TEM), scanning electron microscopy (SEM), high-resolution transmission electron microscopy (HRTEM), BET, Raman spectra, UV–vis diffuse reflectance spectra (DRS), photoluminescence spectra (PLS) and X-ray photoelectron spectroscopy (XPS). XRD, Raman, HRTEM and XPS analysis indicated that WO_x is uniformly dispersed on the surface of TiO_2 probably with monolayer thickness and the mean particle size of the composite was 12 nm. XPS analysis also indicated that the vacuum activated composites contained more W in reduced form while the calcined composites showed more W in hexavalent form. The beneficial effect of W can be explained by considering the formation of W^{+5} species by means of a transfer of photo-generated electrons from TiO_2 to W^{+6}.Subsequently W^{+5} could be oxidized to W^{+6} by transferring electrons to adsorbed O_2.DRS showed an extension of light absorption into the visible region for this WO_x composite and PL analysis indicated that the electron-hole recombination rate has been effectively inhibited when WO_x is deposited on the surface of TiO_2.The samples activated in vacuum showed higher photocatalytic activity than calcined samples in case of MO and superior activity in case of phenol. The optimal WO_3 dosage of 4.0% in WO_x–TiO_2 achieved the highest rate of photodegradation in this experimental condition.

1. Introduction

Among the various nanocrystalline photocatalytic materials that have been studied over the last 30 years, research has mainly focused on titanium dioxide (TiO_2) as photocatalyst in diverse areas ranging from water and air treatment to self-cleaning surfaces. In the past years, TiO_2 has been modified to suit various applications. WO_3/TiO_2 has been successfully tested for selective catalytic reduction (SCR) of NO_x in lean exhaust gases of automobiles to meet the stringent emission standards for both NO_x and particulate matter [1–3]. SiO_2/TiO_2 exhibits super hydrophilic properties that make it an ideal material for antifogging and self-cleaning surfaces such as for window glasses, automobile mirror wind shields, etc. [4]. Numerous papers have appeared on the fundamentals of pure titania systems, the mechanisms of oxidation and the ways to improve its photocatalytic activity (PCA) have been investigated in detail [5–9]. The improvement of the PCA of TiO_2 has been achieved by coating with noble metals such as Ag [10], Au [11], Pt [12] and Pd [13] which can trap the electrons facilitating an effective charge separation. Complementary to metal/TiO_2 photocatalysts, TiO_2 has been coupled with other semiconductors such as SnO_2 [14–17] which can induce effective charge separation by trapping photo-generated electrons. The PCA of metal/metal oxide modified TiO_2 photocatalysts can be further improved if the metal/metal oxide adsorbs more pollutant along with the function of electron trapping. Unfortunately, deposited metal particles only serve as electron trapping agent and are not effective to enhance the adsorption of the pollutants. TiO_2 coupled with other semiconductors has been reported to perform both the above mentioned functions. This has been realized by coupling the WO_3 semiconductor with TiO_2. As a basic function, WO_3 has a suitable conduction band potential to allow the transfer of photo-generated electrons from TiO_2 facilitating effective charge separation. Additionally, formation of a monolayer of WO_x species on TiO_2 can significantly increase the surface acidity as WO_3 is 15 times more acidic than TiO_2[18]. Because of this increased acidity WO_3/TiO_2 can adsorb more hydroxyl groups and simultaneously

* Corresponding author. Fax: +86 21 64252062.
E-mail address: jlzhang@ecust.edu.cn (J. Zhang).

0926-3373/$ – see front matter © 2009 Elsevier B.V. All rights reserved.
doi:10.1016/j.apcatb.2009.06.005

more organic reactants on its surface. Thus, significant improvement of the PCA has been achieved in comparison to the standard commercial photocatalysts. To date, WO_3/TiO_2 has been synthesized by sol–gel [19,20] ball milling [21], incipient wetness impregnation [22,23] and multiple grafting [24]. Thin films of WO_3/TiO_2 have also been produced by dip coating [25] and spin coating [26] Kwon et al. [18] produced WO_3/TiO_2 by wetness impregnation method which includes the suspension of pure TiO_2 powder in a dilute ammonia solution mixed with the required amount of H_2WO_4 to adjust the concentration of WO_3. The resultant powder was then calcined at 400 °C for 2 h. Acidity increased with increasing amount of WO_3 and reached a maximum value for a WO_3 concentration of 3.2 mol%. A further increase in WO_3 concentration did not have any influence on the acidity of WO_3/TiO_2 composite particles. Interestingly, the PCA also followed the same hysteresis as the acidity dependence. Song et al. [23] reported similar results and in addition showed that the stability of the colloidal suspensions of WO_3/TiO_2 was enhanced compared to that of TiO_2 owing to the increased surface acidity. Li et al. [19] synthesized the WO_3/TiO_2 by sol–gel process using ethanol solutions of Ti $(OBu)_4$ and aqueous solutions of ammonium metatungstate. The resultant amorphous WO_x–TiO_2 gel was calcined at 973 K for 2 h to produce crystalline WO_3/TiO_2 nanocomposites. The isoelectric point of the resulting 3 mol% WO_3/TiO_2 composite was found to be at pH 5.0 compared to pH 6.40 for TiO_2. This difference in the isoelectric point can greatly enhance the adsorption of organic components on the WO_x/TiO_2 photocatalysts. All the mentioned synthesis routes involve several processes in order to improve the crystallinity and photo activity of the as synthesized amorphous particles.

In this study the WO_x/TiO_2 composites were synthesized by sol–gel method and activated in a single step thermal treatment in vacuum to enhance the photocatalytic activity in the visible region. During photodegradation of MO under visible light irradiation, this catalyst is much more active than calcined samples while this composite catalyst shows far superior activity to pure TiO_2 in case of phenol. The promoting effects on the activity; the reduced form of tungsten, the surface acidity and the presence of WO_x on the surface of TiO_2 are examined and discussed. To the best of our knowledge this kind of work is performed for the first time.

2. Experimental section

2.1. Chemicals

Tetra butyl titanate (TBT) was used as received. Ammonium tungstate and absolute alcohol were of Analytical grade received from Sinopharm Chemical Reagent Co. Ltd. Shanghai, China and used without any further purification.

2.2. Catalyst preparation

10.0 g of Tetra butyl titanate was dissolved in 7.8 g of absolute alcohol under magnetic stirring, and then ultrasonically dispersed for 20 min to form a homogeneous mixture. 5.0 g of water was slowly dripped into the mixture at a drop rate of 0.5 mL min^{-1} under vigorous stirring, which was stirred further for 1 h at room temperature. Then different additions of ammonium tungstate solution were dripped into the mixture according to the required amount of WO_3 in the nanocomposites. After addition of ammonium tungstate solution, the pH value of the solution was kept to be 10. The solution was aged for 12 h at ambient temperature, followed by filtering, washing for several times with deionised water and absolute alcohol, drying at 353 K for 12 h to produce a precursor.

Pure TiO_2 was also prepared by the same procedure without the addition of ammonium tungstate. Subsequently the products were activated in vacuum at 470 K for 2 h resulted in the formation of WO_x/TiO_2 nanocomposites. The calcined products were prepared at 673 K in air for 5 h to compare with the evacuated samples.

2.3. Characterization

UV–vis diffuse reflectance spectrum (DRS) was obtained with a Scan UV–vis–NIR spectrophotometer (Varian Cary 500) equipped with an integrated sphere assembly, using $BaSO_4$ as a reflectance sample. X-ray diffraction (XRD) measurements were carried out to investigate the crystallographic properties with a Rigaku D/Max 2550 VB/PC apparatus (Cu Kα radiation, λ = 1.54056 Å) at room temperature operated at 40 kV and 100 mA. Diffraction patterns were recorded in the angular range of 20–80°. The Scherrer equation was applied to estimate the average crystallite sizes of TiO_2 samples;

$$D = \frac{K\lambda}{\beta\cos\theta}$$

Where β is the half-height width of the diffraction peak of anatase (101), $K = 0.89$ is a coefficient, θ is the diffraction angle, and λ is the X-ray wavelength corresponding to the Cu Kα radiation. D is the average crystallite size of the powder sample in nanometer. Raman spectrum of the sample was recorded by Renishaw inVia Raman spectrometer at room temperature with the excitation wavelength of 514.6 nm. The surface morphologies and particle sizes were observed by scanning electron microscopy (JEOL.JSM-6360LV) and high-resolution transmission electron microscopy (JEOL.JEM-2011), using an accelerating voltage of 200 KV. The samples were supported on carbon-coated copper grids for HRTEM. The S_{BET} of the samples were determined through nitrogen physical adsorption at 77 K (Micromeritics ASAP 2010). All the samples were degassed at 473 K before the measurement.

To investigate the chemical states of the photocatalysts, X-ray photoelectron spectroscopy (XPS) was recorded with PerkinElmer PHI 5000C ESCA System with Al Kα radiation operated at 250 W. The shift of binding energy due to relative surface charging was corrected using the C 1s level at 284.6 eV as an internal standard.

Photoluminescence spectra (PLS) were recorded by Varian Cary Eclipse Fluorescence spectro photometer with Varian Cary under the excitation light at 270 nm. The UV–vis absorption spectra of the samples were recorded on Cary 100 UV/vis spectrophotometer.

The pure sample of phenol and samples after irradiation in visible light are quantified by HPLC (all compounds were verified by use of authentic samples in HPLC). The HPLC series 1100 (Agilent) is equipped with a reverse-phase C18 analytical column of 150 mm × 2.1 mm and 3.5 μm particle diameter. Column temperature was maintained at 22 °C. The mobile phase used for eluting phenol from the HPLC columns consisted of acetonitrile and water (30:70, v/v) at a flow-rate of 0.3 mL min^{-1}.

For the measurement of surface acidity, each sample (0.1 g) was suspended in benzene and then titrated with n-butylamine benzene solution, using methyl red as an indicator.

2.4. Photocatalytic activity test

After characterization, the photocatalytic performance of WO_x/TiO_2 nanocomposites was evaluated in comparison with the vacuum activated and calcined samples in the degradation of methyl orange. The photocatalytic activity of vacuum activated samples was also checked for the degradation of phenol in visible light. The first one is representative of dyes, while phenol is a highly persistent pollutant. We studied their photocatalytic

degradation processes on exposure to visible light. The photocatalytic degradation was carried out in a 100 mL quartz photochemical reactor. The initial concentration of MO and phenol in a quartz reaction vessel was fixed at 40 and 30 mg L^{-1} respectively, with a catalyst loading of 1.0 g L^{-1}. A 1000 W halogen lamp was used as the light source and the light from the lamp included beams from ultraviolet and visible light regions. The short-wavelength components ($\lambda < 420$ nm) of the light were cut-off using a cut-off glass filter. During the reaction, a water-cooling system cooled the water-jacketed photochemical reactor to maintain the solution at room temperature. The distance between the lamp and the centre of quartz tube was 10 cm. Prior to illumination, the suspension was magnetically stirred in darkness for 30 min to establish adsorption–desorption equilibrium at room temperature. During irradiation, stirring was maintained to keep the mixture in suspension. At regular intervals, samples were withdrawn and centrifuged to separate photocatalyst for analysis. Then filtered through a 0.22 u.m Millipore filter to remove the photocatalyst. The photoactivities for MO and phenol in dark in the presence of the photocatalyst and under visible light irradiation in the absence of the photocatalyst were also evaluated. The extent of MO decomposition was determined by measuring the absorbance value at approximately 465 nm. The concentration of phenol was calculated from the height of peak at 270 nm by using the calibration curve. The measurements were repeated for the catalyst and the experimental error was found to be within ±3%. During photocatalytic degradation of phenol, reaction mixture was sonicated for 20 min to homogenize. The photoreactor was continuously purged with air at a flow-rate of 100 mL min^{-1} to guarantee sufficient O_2 concentration in the reaction medium.

3. Results and discussion

3.1. UV–vis diffused reflectance spectra (DRS)

As shown in Fig. 1a, the UV–vis diffuse reflectance spectrum (DRS) of pure TiO_2 sample is dominated by the edge relative to the O^{-2}–Ti^{+4} charge transition at 300–380 nm of TiO_2 anatase which agrees well with the results quoted [27,28]. These charge transitions correspond to the excitation of electrons from the valence band to the conduction band. In Fig. 1b, the 4.0% WO_x/TiO_2 calcined composite shows an additional broad and weak absorption in the visible region in the range of 400–500 nm. This absorption, responsible for the pale yellow color of the samples, can be due to a O^{-2}–W^{+6} charge transfer transition [29], as in case of monoclinic WO_3[30]or to a perturbation of the TiO_2 edge by surface tungsten oxide species. The absence of significant absorptions in the visible region due to d–d transition points to the absence of reduced W species with respect to the d_0 hexavalent state in the calcined samples. However, in Fig. 1c the spectrum of 4.0% composite activated under vacuum at 470 K for 2 h shows an additional broad absorption that extends throughout all the visible region, that is not observed in the case of pure TiO_2 and WO_x/TiO_2 composite calcined at 673 K. This absorption, responsible for the dark brown color of the evacuated materials, is associated with the reduction of W^{+6} [31] to a lower oxidation state W^{+5}.

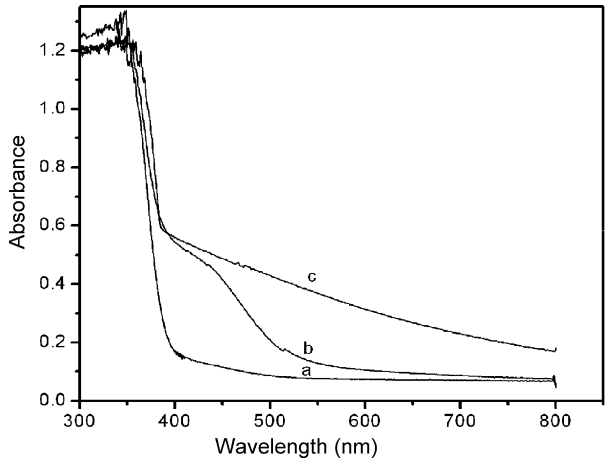

Fig. 1. UV–vis diffused reflectance spectra of various samples (a) TiO_2. (b) 4.0%WO_x/TiO_2 calcined composite (c) 4.0%WO_x/TiO_2 activated in vacuum.

3.2. X-ray diffraction (XRD)

The phase structure, crystallite size and crystallinity of TiO_2 play important roles in photocatalytic activity and many studies have confirmed that anatase phase of titania shows higher photocatalytic activity than brookite or rutile phase [32]. XRD was used to investigate the changes of phase structure of TiO_2 samples prepared with different ammonium tungstate addition. The XRD patterns of the samples are shown in Fig. 2. It can be seen that the diffraction peaks of all samples are ascribed to the peaks of TiO_2 anatase phase [JCPDS No.21-1272]. As seen in the inset Fig. 2, if compared to the pure TiO_2, the peak width at $2\theta = 25.3^\circ$ in all the composites is much broader. It is worth noting that no tungsten oxide phase could be observed, even the amount reaches 4.0%. The reason is that it is present either in the form of highly dispersed WO_x monolayer or as an amorphous layer on TiO_2 as reported by several authors [21] or the concentration of tungsten oxide is too low for the XRD to reveal. In contrast, reflections corresponding to crystalline WO_x are seen in the XRD pattern of nanocomposites synthesized at higher wt. % WO_x/TiO_2. The average size of TiO_2 crystallites was estimated based on the broadening of anatase (101) peak at $2\theta = 25.3^\circ$ using the Scherrer equation [33]. Structure analysis of the WO_x–TiO_2 with different tungsten loading contents suggests the anatase phase and the particle size of all the as-prepared TiO_2 is 10–15 nm. Engweiler et al. [24] studied the formation of WO_3/TiO_2 composites via multiple grafting procedures by step-wise increase of the concentration of WO_x species and concluded that a highly dispersed amorphous monolayer of WO_x species forms on TiO_2 at low tungsten loading. When the tungsten concentration exceeds over that required for WO_x monolayer formation, crystalline WO_x will form. After the wt. percentage of tungsten oxide in TiO_2 reaches at higher level, the peaks of WO_x start to appear in the XRD patterns of WO_x/TiO_2. Ma

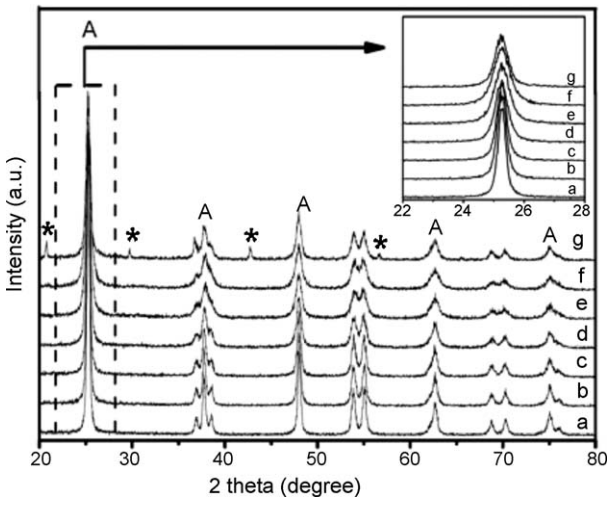

Fig. 2. XRD patterns of different samples: (a) TiO_2, (b) 1.0%WO_x/TiO_2, (c) 2.0%WO_x/TiO_2, (d) 3.0%WO_x/TiO_2, (e) 4.0%WO_x/TiO_2, (f) 5.0% WO_x/TiO_2, (g) 6.0% WO_x/TiO_2.

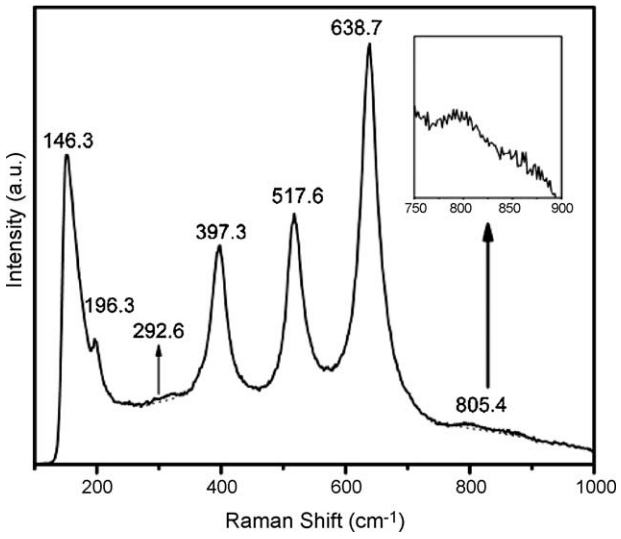

Fig. 3. Raman spectrum of 4.0% WO_x/TiO_2.

et al. [34] also reported the same results in their studies, they thought that amorphous tungsten oxide phase covered the TiO_2 surface. Similar observations have been made in the present study with the increased concentration of tungsten oxide. The results show that when the amount of WO_x decorated is less, a highly dispersed amorphous monolayer of WO_x species forms on TiO_2. But when the amount of WO_x is high, the diffraction peaks of WO_x can be found in XRD patterns.

3.3. Raman spectra

The laser Raman spectrum of 4.0% WO_x/TiO_2 sample is shown in Fig. 3. The Raman bands of TiO_2 appeared at 146.3,196.3, 397.3,517.6 and 638.7 cm^{-1}. The bands typical of anatase are observed at 146.0, 196.0, 397.0, 516.0 and 638.0 cm^{-1} [35] assigned to the E_g, B_{1g}, A_{1g}, B_{2g}, and E_g vibrational modes of TiO_2, respectively and these results are consistent with the XRD measurements The peaks which are associated with tungsten species, WO_3 show very weak absorptions at 270, 293, 325 cm^{-1}, responsible for typical sharp Raman bands in the regions 700–900 cm^{-1} are not detected. Two weak bands appear at 292.6 and 805.4 cm^{-1} in 4.0% WO_x/TiO_2 sample. As seen in inset Fig. 3, the composite shows very weak band at 805.4 cm^{-1}.The Raman spectra are similar to those reported in the literature for WO_3/TiO_2 catalysts [37,38]. Raman spectra confirm inferences from XRD data that WO_3 is not present as a separate phase. This result, suggests that tungsten oxide spreads over the TiO_2 surface, would be expected at the low W loading of this sample, that is, according to literature data [36,39].

3.4. SEM and TEM observation

The SEM image shown in Fig. 4a, providing visualization of the textural properties of large portions of sample, indicates that the composite is made up of irregular-shaped, loose aggregates with a significant quantity of interparticle voids. TEM observation in Fig. 4b reveals that the 4.0% WO_x–TiO_2 sample consists of agglomerates of primary particles of 10–15 nm in diameter, which is in general agreement with the XRD determination. HRTEM in Fig. 4c, the high-resolution image of the optimized 4.0% WO_x/TiO_2 particles shows uniform lattice fringes whose spacing corresponds to (101) planes of anatase phase of TiO_2 and no individual clusters/particles of tungsten oxide are seen on the surface of TiO_2 [18,23]. This indicates that the tungsten oxide species might have covered the surface of TiO_2 particles as amorphous layer. This is consistent with the results obtained from the Raman spectroscopy and XRD showing the existence of amorphous WO_x and agrees well with previous reports.

3.5. BET-surface areas

As shown in Table 1, all samples have large surface areas, which may contribute to the high photocatalytic activities of the samples. The N_2 adsorption–desorption isotherms of pure TiO_2, 2.0 wt% WO_x/TiO_2, 3.0 wt% WO_x/TiO_2 and 4.0 wt% WO_x/TiO_2 are shown in Fig. 5. All the samples show similar N_2 adsorption and desorption isotherms. According to IUPAC [40] it is seen that the adsorption isotherm belongs to Type II, while the desorption isotherm belongs to Type IV. Therefore it can be concluded that the particle size of the prepared samples was mainly distributed in the mesoporous range [41]. A clear hysteresis loop at high relative pressure is observed, which is related to the capillary condensation association with large pore channels. The pore size distribution of the prepared samples was approximately 2.7–3.2 nm according to the BJH solutions of the desorption curves.

3.6. Photoluminescence spectra (PLS)

Photoluminescence spectra have been widely used to investigate the efficiency of charge carriers trapping, immigration and transfer, and to understand the fate of electrons/hole pairs in semiconductor particles [42]. Fig. 6 demonstrated that both TiO_2 and composite samples exhibited the PLS peaks. In this study, the PL spectra of all samples were examined in the wavelength range of 350–500 nm. It is observed that PL spectra of the pure TiO_2 are higher in intensity than that the spectra of WO_x–TiO_2 sample. The

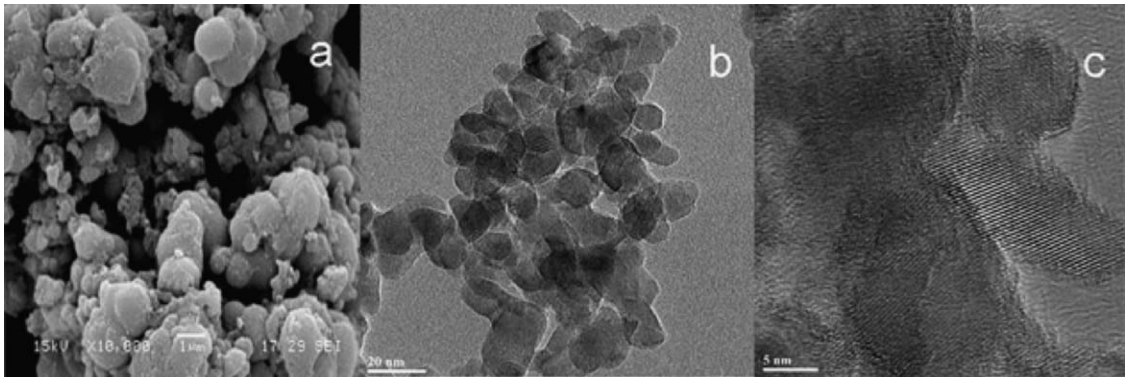

Fig. 4. SEM, TEM and HRTEM micrographs of 4.0% WO_x/TiO_2 (a–c).

Table 1
The crystal sizes and BET surface area of different samples.

Sample	Particle size (nm)[a]	S_{BET} (m^2/g)	Pore Size (nm)
TiO_2	16	186	2.7
2.0% WO_x/TiO_2	14	280	2.8
3.0% WO_x/TiO_2	13	350	2.9
4.0% WO_x/TiO_2	12	392	3.2

[a] Determined by XRD using Scherrer equation.

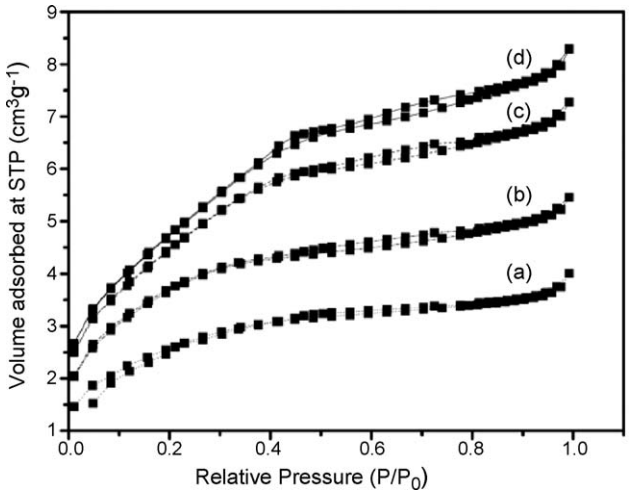

Fig. 5. N_2 adsorption–desorption isotherms (a) Pure TiO_2; (b) 2.0% WO_x/TiO_2(c) 3.0% WO_x/TiO_2 (d) 4.0% WO_x/TiO_2.

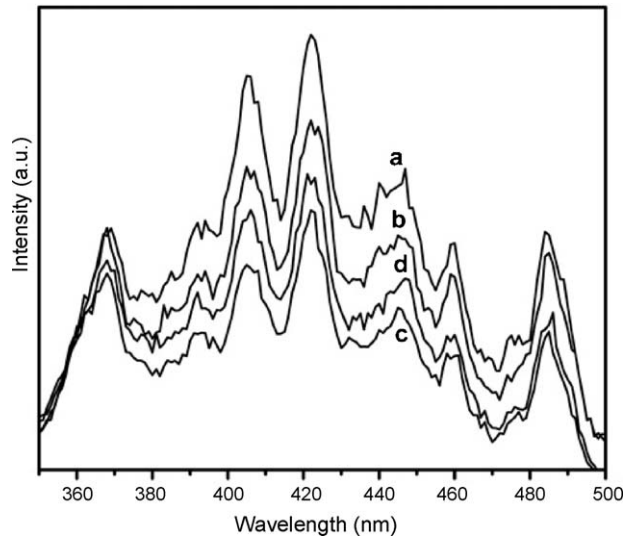

Fig. 6. Photoluminescence spectra of various samples (a) TiO_2, (b) 2.0% WO_x/TiO_2, (c) 4.0% WO_x/TiO_2, (d) 5.0%WO_x/TiO_2.

PL intensity greatly decreased due to the decorating tungsten oxides although the PL intensity increased back when the content of tungsten oxides exceeded 4.0% because of the presence of more tungsten oxide. The observed PL spectra are attributed to the radioactive recombination process of either self-trapped excitons [43,44] or hydroxylated Ti^{+3} surface complexes [45] from the charge transfer excited state of the highly dispersed TiO_2 species. However, in this study there was no any fitting peak of Ti^{+3} for the 4.0% WO_x–TiO_2 found in the XPS analysis. Then, the reduction of PL intensity indicates the decrease of radioactive recombination process. The experimental results demonstrated that PL spectra are quite sensitive to the amount of tungsten oxide. The variation of PL intensity may result from the change of defect state on the shallow level of TiO_2 surface [46]. Fig. 6 also shows the comparison of the photoluminescence spectra for blank TiO_2 and WO_3 coated TiO_2 nanoparticles. As for the blank TiO_2, the well resolved peaks/shoulders at 392, 398, 424, 451, 461 and 486 were observed. All these peaks/shoulders are ascribed to surface traps [47–49]. On the basis of the relevant band positions of tungsten oxide and TiO_2, photo-generated electrons are transferred from TiO_2 conduction band to the tungsten oxide conduction band and the holes accumulate in the TiO_2 valence band. Hence, photo-generated electrons and holes were efficiently separated. On the other hand, when the contents of tungsten oxide were lower than its optimal ratio, tungsten energy level would be a separation centre. On the contrary, when the content of tungsten oxides was higher than its optimal ratio, tungsten energy level would be a recombination centre.

3.7. XPS spectra

XPS measurements were performed to elucidate the surface chemical composition and the oxidation state for the WO_x/TiO_2 composites. Fig. 7 indicates XPS survey spectra for the WO_x/TiO_2 composites and pure TiO_2. The XPS analysis indicate that the WO_x/TiO_2 composites contain Ti, W, O, and trace amounts of carbon, which originates from the residual carbon in the composite and the adventitious hydrocarbon in the XPS instrument itself.

The XPS analysis elucidate that the W is present on surface of TiO_2 and during vacuum activation, Ti^{+3} species are generated by Ti^{+4}, the electron is transferred from the conduction band of TiO_2 to the lower-lying conduction band of WO_3 to reduce the W^{+6} to W^{+5} and the Ti^{+3} are oxidized to Ti^{+4} by losing the electron. So the Ti^{+3} species are oxidized to Ti^{+4}. XPS data further confirmed that there is no fitting peak of Ti^{+3}. This is evidence that WO_3 is not impregnated into TiO_2, but is just loaded on the surface of TiO_2 particles.

The binding energies (B.E) of Ti $2p_{3/2}$ and Ti $2p_{1/2}$ of pure titania were 458.1 and 463.8 eV, respectively, and are attributed to Ti^{4+} [50]. Different wt. % of composite also showed the same binding energies. With the incorporation of W species, the intensity of Ti 2p was decreased. This also suggests that relatively W species are present on the surface of the TiO_2 [64]. Presence of tungsten oxide on the surface of TiO_2 did not alter the Ti 2p binding energies as shown in Fig. 7a. In Fig. 7b, the O 1s band of pure TiO_2 and the WO_x/TiO_2 composite showed the same binding energy at 529.6 e V. Therefore, it can be concluded that no obvious changes on the chemical state of Ti and O can be caused by the presence of WO_x species on the surface of TiO_2. As the % of tungsten oxide increased to 5.0 wt%, the O 1s of WO_x/TiO_2 became broad. This may be due to the adsorption of more water or hydroxyl groups. In the present work, energy levels of tungsten were measured in the W4f $_{5/2}$ regions of 4.0% WO_x/TiO_2 composite activated in vacuum and calcined in air as shown in Fig. 7c and d respectively. According to the curve fit data of W4f $_{5/2}$ of 4.0% composite activated in vacuum as shown in Fig. 7c, showed the binding energies of W (V) 36.1 and W (VI) 37.8 eV [51–53]. While the percentages of W (V) and W (VI) were found to be 60.2 and 39.8% respectively. While curve fit data of 4.0% calcined composite showed the approximately same binding energies of W (VI) 37.8 eV and W (V) 36.2 eV but the percentages of W (VI) and W (V) were found to be 64.7 and 35.3% respectively. It is concluded that 4.0% WO_x/TiO_2 composite activated in vacuum contains more reduced tungsten (V) oxide than tungsten (VI) oxide while 4.0% WO_x/TiO_2 calcined composite contains more tungsten (VI) oxide. According to the curve fit data of W4d $_{5/2}$ of 4.0% composite activated in vacuum as shown in Fig. 7e, similar results were observed by the presence of W4d $_{5/2}$ with binding energies of 246.8 and 248.2 eV respectively [54]. This also confirmed the presence of more reduced form tungsten (V)

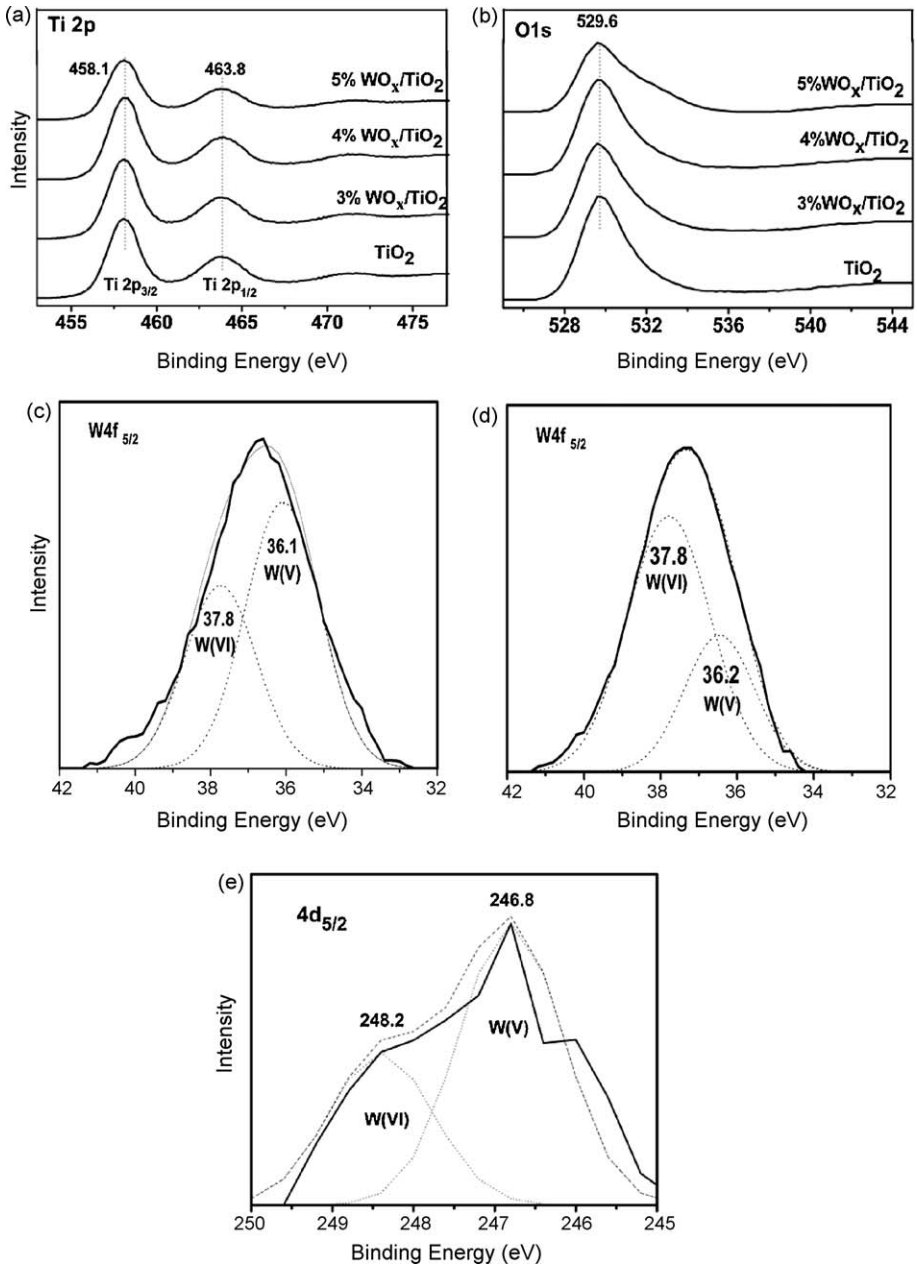

Fig. 7. XPS spectra of various samples: (a) Ti 2p. (b) O 1s of TiO_2 and WO_x/TiO_2 composites (c)W 4f of 4.0% evacuated composite (d)W 4f of 4.0% calcined composite (e)W 4d of 4.0% evacuated composite.

oxide which is in good agreement with the results quoted in the literature given above.

3.8. Photocatalytic degradation of organic compounds

The photo degradation of organic compounds is employed to evaluate the photocatalytic activities of pure TiO_2 and the composite catalysts. It was observed that the composite showed high activity in the degradation of MO and phenol under visible light when it has been activated in vacuum. The highest activity of the vacuum activated samples is observed at 4.0% wt. tungsten loading and about 83.0% of MO was degraded after reaction for 5 h under visible light in WO_x/TiO_2 suspension as shown in Fig. 8a, while the calcined samples showed 25.0% under same experimental conditions as seen in Fig. 8b. The vacuum activated samples showed three times more activity than calcined samples. The presumed reason is that the absorptions in vacuum activated samples are associated with the reduction of W^{+6} to a lower oxidation state W^{+5}.Subsequently W^{+5} oxidized to W^{+6} by transferring electrons to adsorbed O_2.While in calcined samples there is absence of significant absorptions in the visible region due to d–d transition points to the absence of reduced W species with respect to the d_0 hexavalent state [31]. Fig. 9a illustrated that 68.0% of phenol was degraded after reaction for 5 h under visible light in WO_x/TiO_2 suspension. 4.0 wt. % WO_x/TiO_2 novel photocomposite showed the best activity and demonstrated to be far superior to that of pure TiO_2. These results are in agreement with those obtained previously using impregnated [55] and sol–gel prepared powders [56]. The beneficial effect of W has been explained [57] by considering the formation of W (V) species. Subsequently W (V) could be oxidized to W (VI) by transferring electrons to adsorbed O_2. The vacuum activated samples contain more reduced form W^{+5} while the calcined samples have more W^{+6} as concluded by XPS data. It is observed that 55.0% of phenol was degraded after

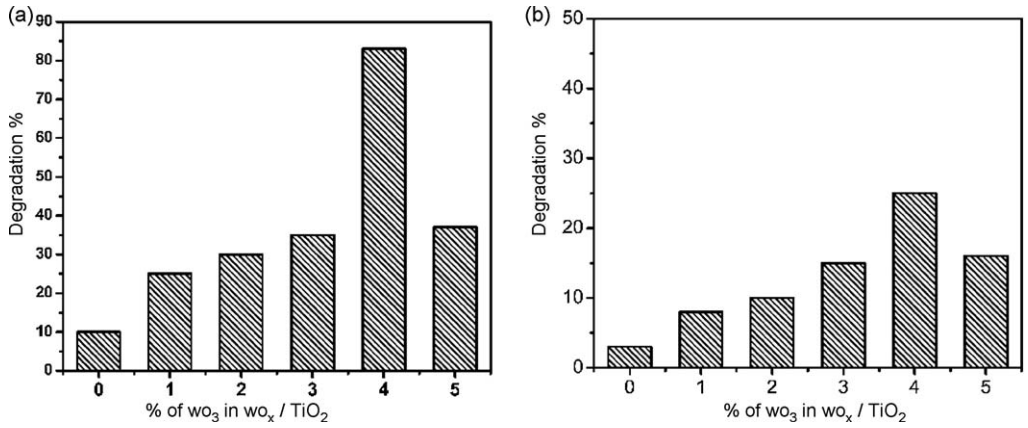

Fig. 8. Photocatalytic degradation of methyl orange under visible light illumination for 5 h. (a) samples activated in vacuum; (b) calcined samples.

reaction for 5 h under UV light in WO_x/TiO_2 suspension. 4.0 wt. % WO_x/TiO_2 novel photocomposite showed better activity than TiO_2 and the pure TiO_2 showed 20.0% activity in the degradation of phenol in UV. It is known that band gaps of WO_3 and TiO_2 are 2.8 and 3.2 eV, respectively. TiO_2 can be excited by photons with wavelengths under 387 nm, which produces photo-generated electron-hole pairs and show photocatalytic activity. But when WO_3 and TiO_2 form a coupled photocatalyst, TiO_2 and WO_3 can be excited simultaneously under UV illumination. As the conduction band of WO_3 is lower than that of TiO_2, the former can act as a sink for the photo-generated electrons. The photo-generated electrons of the TiO_2 conduction band will be transferred to the conduction band of WO_3. Since the holes move in the opposite direction from the electrons, photo-generated holes might be trapped within the TiO_2 particle, which makes charge separation more efficient. The result is that the WO_x/TiO_2 coupled photocatalyst exhibits even higher photocatalytic activity than that of TiO_2 which has good agreement with the results quoted [58,59,61].

The recombination of photo-generated electrons and holes is one of the most significant factors that influence the photo activity of the samples. When WO_3 and titania form a composite photocatalyst, the photo excitation process occurs. The photo-generated electrons can be transferred to the lower-lying conduction band of tungsten oxide, while the holes will accumulate in the valence band of titania, and effectively scavenged by the oxidation, while the photo-generated electrons can be transferred onto the surface of tungsten oxide rather than undergoing bulk recombination [60]. When $W^{+5}O_x$ form the composite catalyst, similar process occurs but it can reduce the band gap more and the recombination of electron-hole is more difficult as shown in Scheme 1.The purpose of Scheme 1 is to compare the band gap energy of the composite activated in vacuum and in calcined samples. The band gap between the new states and the conduction band is lower in vacuum activated sample than calcined composite. Thus it makes the vacuum composite highly active in visible light as compared to calcined samples. The formed W^{+5} then can transfer the electrons to surface reducible species to improve the photocatalytic activity. These processes promote the separation of the photo-generated electrons and holes to accelerate the process. At the same time, the composite shows red shift in the absorption wavelength range compared with that of TiO_2, which might be also benefit for the improvement of the photocatalytic performance of the composite materials.

$$W^{+6} + e^- \rightarrow W^{+5}$$

As reported before, a WO_3/TiO_2 film with monolayer coverage of WO_3 on the surface of TiO_2 nanoparticles has also shown better photocatalytic performances than that of the pure TiO_2 film, they think that the higher activity of WO_3/TiO_2 film can be ascribable to the higher acidity and affinity for chemical species. It is well known that WO_3 retains a much higher Lewis surface acidity than TiO_2 and has a higher affinity for chemical species having unpaired electrons. Table 2 shows the acidity of WO_3/TiO_2 as a function

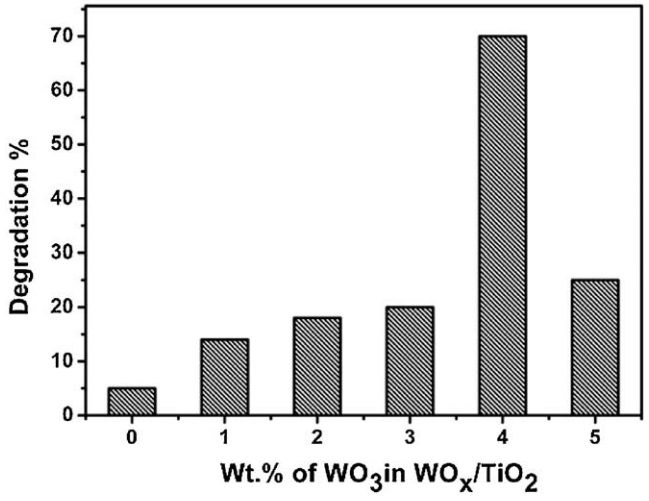

Fig. 9. Photocatalytic degradation of phenol under visible light illumination for 5 h.

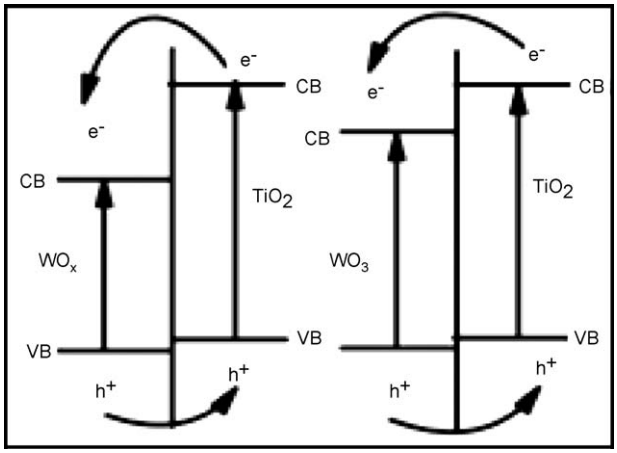

Scheme 1. Mechanism of WO_x (Vacuum activated) and WO_3 (Calcined) composite excitation process.

Table 2
The surface acidity of pure TiO_2 and different composite samples.

Sample	Surface acidity(mmolg^{-1})
TiO_2	0.09
1.0% WO_x/TiO_2	0.17
2.0% WO_x/TiO_2	0.24
3.0% WO_x/TiO_2	0.29
4.0% WO_x/TiO_2	0.33
5.0% WO_x/TiO_2	0.32
6.0% WO_x/TiO_2	0.32

of the WO_3 composition. By the incorporation of WO_3, the surface acidity of the resultant structures was considerably increased due to the highly acidic nature of WO_3. For the initial addition of WO_3, especially the introduction of 1.0, 2.0 and 4.0 wt % WO_3, the surface acidity increases from 0.17 to 0.24 and 0.33 mmol/g, respectively. However, with a higher concentration of WO_3 over 5 and 6 wt. %, the surface acidity was not appreciably changed. This result was similar to the previous reports on the surface modification of TiO_2 particles with WO_3 [62,63]. The other factor influencing the photocatalytic efficiency is the high adsorption affinity of WO_3/TiO_2. It was found that by loading 4.0% of WO_3 on TiO_2 particles, the Lewis surface acidity was increased much. Thus the WO_3/TiO_2 particles can adsorb more OH^- or H_2O on the surface and generate a greater amount of OH radicals. At the same time, WO_x/TiO_2 particles have a higher adsorption affinity toward the reactant molecules. It has also been observed that 4.0% showed the highest adsorption i.e. 15.0% and as well as the photoactivity. TheWO_x/TiO_2 particles with high Lewis surface acidity are much more hydrophilic than pure TiO_2. Thus, the stability of their suspension could be improved. This indicates that WO_x/TiO_2 samples are more stably suspended in water than pure TiO_2.This may have an influence on the photocatalytic activity of WO_3/TiO_2. These results agree well with the results quoted [18,23]. The enhanced photocatalytic activity of the present 4.0% WO_x/TiO_2 nanocomposites can also partially be ascribed to the similar reason which agrees well with the results quoted [64]. Moreover, the increased specific surface area and finer particle size of 4.0% WO_x/TiO_2 as shown in Table 1 may be another reason to enhance the photocatalytic behavior of tungsten oxide modified TiO_2 [65]. The differences in photo activity between TiO_2 and loaded samples can be also attributed to other characteristics such as the larger particle size. Tanabe [66–68] has studied that the presence of a second metal oxide in contrast with TiO_2, such as WO_3/TiO_2 should cause an increase in acidity. When the loaded WO_3 exceeds 5.0 wt%, the photocatalytic activity of the composite decreases even though the visible light absorption still increases. It may be the charge transfer of the composite catalysts to O_2 or target molecules could be retarded with too much WO_3 coupling [69].

The photocatalytic oxidation of phenol involves complicated multistage processes as shown in Scheme 2. It has been demonstrated that the photocatalytic process with titania is energetically favorable for the decomposition of phenolic compounds and that two types of oxidizing species hydroxyl radicals and positive holes are involved in the transformation of aromatic compounds in oxygenated aqueous titania suspensions [70,71]. Various aromatic intermediates products were formed in the initial stage. The intermediate products then undergo further photocatalytic oxidation to induce ring cleavage to form aliphatic acids, and finally, they completely degrade to CO_2 and H_2O.

However, HPLC results as shown in Fig. 10, obtained in the present study indicate that the reactions catalyzed by the WO_x/TiO_2 products followed the same degradation pathway mentioned

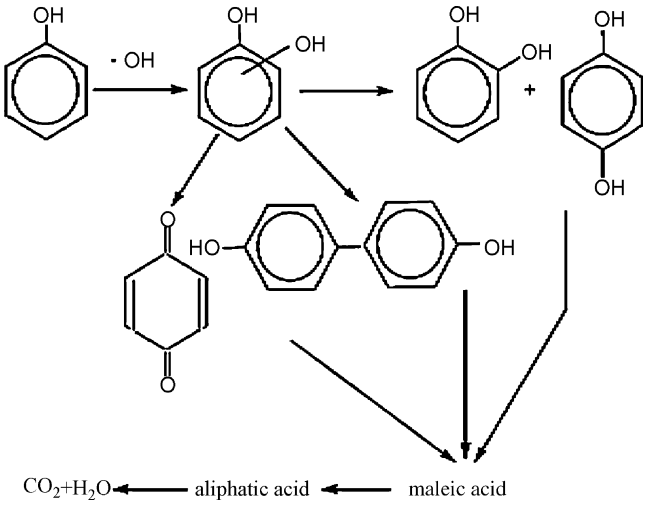

Scheme 2. Phenol degradation with reaction pathway during the photocatalytic reaction.

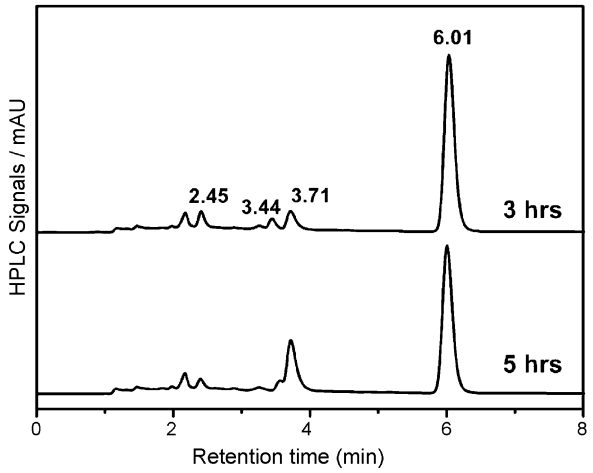

Fig. 10. HPLC data of photocatalytic degradation of phenol over 4.0%sample activated in vacuum.

in Scheme 2. In the degradation of phenol with retention time RT 6.01 min, the dihydroxybenzene RT 3.44 min, benzoquinone RT2.45 min, and maleic anhydride RT3.71 min, were the main intermediates identified. Polar compounds such as carboxylic acid eventually degraded to CO_2 [72,73]. Further degradation of the intermediates was likely via several reaction pathways (including oxidative hydroxylation, ring cleavage, oxidative decarboxylation, etc.) that were simultaneously operative. The photodegradation pathways proposed in Scheme 2 are consistent with the results of other research groups with anatase titania nanoparticles as catalyst [74–76]. For example, Azevedo reported that three compounds, catechol, hydroquinone, and 4, 4′-dihydroxybiphenyl were formed during photodegradation in function of salinity [74] Catechol, hydroquinone, and 1, 2, 3-trihydroxybenzene were identified as primary and secondary hydroxylation products [70]. 1, 2, 4-trihydroxybenzene and benzoquinone have also been reported as the intermediate species during phenol mineralization [71].

Under different reaction conditions, the primary aromatic intermediates could be different. For example, during oxidation of phenol in alkaline medium, catalyzed by PCS, p-benzoquinone is one of the primary intermediate products. The p-benzoquinone was easily oxidized in alkaline solution [74–76].

4. Conclusions

The WO_x/TiO_2 composites with different contents of tungsten oxide have been prepared by sol–gel method reported here. These samples are characterized by different methods including XPS, SEM, TEM, HRTEM, XRD, BET surface area, Raman, DRS and PLS measurements. The evacuated samples have dark brown color while the calcined samples have light yellow color. Vacuum activated WO_x/TiO_2 nanocomposites exhibit higher photocatalytic activity than calcined samples, and the optimum % of WO_3 in WO_x/TiO_2 is 4.0 wt %. Phenol and MO have been successfully degraded in visible light. The degradation of phenol is further confirmed by the formation of intermediates by HPLC data. The monolayer coverage of WO_x promotes the separation of photo-generated carriers. The increased photocatalytic activity of the coupled nanocomposites is attributed to the increased surface acidity, the charge separation efficiency, the extension of the wavelength range of photo excitation and reduction of W^{+6} to a lower oxidation state W^{+5}. The higher BET surface areas and finer particle sizes also contribute in this. Thus the composite showed higher photo activity under visible light due to the single step activation under thermal treatment in vacuum.

Acknowledgments

This work has been supported by Science and Technology Commission of Shanghai Municipality (07JC14015); Shanghai Nanotechnology Promotion Centre (0752nm001), National Nature Science Foundation of China (20773039, 20577009); National Basic Research Program of China (973 Program, 2007CB613306, 2004CB719500), and the Ministry of Science and Technology of China (2006AA06Z379, 2006DFA52710). Sajjad Ahmed Khan Leghari and Shamaila Sajjad thank Higher Education Commission (Pakistan) for support.

References

[1] J.M. Herrmann, J. Disdier, J. Catal. Today 56 (2000) 389–401.
[2] S. Djerad, L. Tifouti, M. Crocoll, W. Weisweiler, J. Mol. Catal. A: Chem. 208 (2004) 257–265.
[3] S.T. Choo, S.D. Yim, I.-S. Nam, S.-W. Ham, J.-B. Lee, Appl. Catal. B: Environ. 44 (2003) 237–252.
[4] T. Watanabe, S. Fukayama, M. Miyauchi, A. Fujishima, K. Hashimoto, J. Sol–Gel Sci. Technol. 19 (2000) 71–76.
[5] P.V. Kamat, Chem. Rev. 93 (1993) 267–300.
[6] A. Hagfeldt, M. Graetzel, Chem. Rev. 95 (1995) 49–68.
[7] A.L. Linsebigler, G. Lu, J.T. Yates, Chem. Rev. 95 (1995) 735–758.
[8] M.R. Hoffmann, S.T. Martin, W. Choi, D.W. Bahnemann, Chem. Rev. 95 (1995) 69–96.
[9] M.A. Fox, M.T. Dulay, Chem. Rev. 93 (1993) 341–357.
[10] T. Hirakawa, P.V. Kamat, Langmuir 20 (2004) 5645–5647.
[11] M. Jakob, H. Levanon, P.V. Kamat, Nano Lett. 3 (2003) 353–358.
[12] T. Johannessen, S. Koutsopoulos, J. Catal. 205 (2002) 404–408.
[13] T. Sano, S. Kutsuna, N. Negishi, K. Takeuchi, J. Mol. Catal. A: Chem. 189 (2002) 263–270.
[14] K. Vinodgopal, I. Bedja, P.V. Kamat, Chem. Mater. 8 (1996) 2180–2187.
[15] K.K. Akurati, A. Vital, R. Hany, B. Bommer, T. Graule, M. Winterer, Int. J. Photoenergy 7 (2005) 153–161.
[16] B. Pal, T. Hata, K. Goto, G. Nogami, J. Mol. Catal. A: Gen. 169 (2001) 147–155.
[17] L. Spanhel, H. Weller, A. Henglein, J. Am. Chem. Soc. 109 (1987) 6632–6635.
[18] Y.T. Kwon, K.Y. Song, W.I. Lee, G.J. Choi, Y.R. Do, J. Catal. 191 (2000) 192–199.
[19] X.Z. Li, F.B. Li, C.L. Yang, W.K. Ge, J. Photochem. Photobiol. A: Chem. 141 (2001) 209–217.
[20] H. Yang, R. Shi, K. Zhang, Y. Hu, A. Tang, X. Li, J. Alloys Compd. 398 (2005) 200–202.
[21] C. Shifu, C. Lei, G. Shen, C. Gengyu, Powder Technol. 160 (2005) 198–202.
[22] Y.R. Do, W. Lee, K. Dwight, A. Wold, J. Solid State Chem. 108 (1994) 198–201.
[23] K.Y. Song, M.K. Park, Y.T. Kwon, H.W. Lee, W.J. Chung, W.I. Lee, Chem. Mater. 13 (2001) 2349–2355.
[24] J. Engweiler, J. Harf, A. Baiker, J. Catal. 159 (1996) 259–269.
[25] A. Rampaul, I.P. Parkin, S.A. O'Neill, J. DeSouza, A. Mills, N. Elliott, Polyhedron 22 (2003) 35–44.
[26] T. Tatsuma, S. Takeda, S. Saitoh, Y. Ohko, A. Fujishima, Electrochem. Commun. 5 (2003) 793–796.
[27] D.N. Ke, H.J. Liu, T.Y. Peng, X. Liu, K. Dai, Mater. Lett. 62 (2008) 447–450.
[28] X. Ding, X.G. Xu, Q. Chen, L.M. Peng, Nanotechnology 17 (2006) 5423–5427.
[29] A. Gutiérrez-Alejandre, P. Castillo, J. Ramírez, G. Ramis, G. Busca, Appl. Catal. A: Gen. 216 (2001) 181–194.
[30] G. Ramis, C. Cristiani, M.S. Elmi, P.L. Villa, G. Busca, J. Mol. Catal. 61 (1990) 319.
[31] G. Ramis, G. Busca, C. Cristiani, L. Lietti, P. Forzatti, F. Breganis, Langmuir 8 (1992) 1744–1749.
[32] O. Carp, C.L. Huisman, A. Reller, Prog. Solid Sate Chem. 32 (2004) 33–177.
[33] G.V. Vasilenko, V.I. Zarembo, A. Slobodov, A. Russ, J. Appl. Chem. 70 (1997) 1498–1502.
[34] Z. Ma, W. Hua, Y. Tang, Chem. Lett. 28 (1999) 1215–1224.
[35] I.R. Beattie, T.R. Gilson, J. Chem. Soc. A (1969) 2322–2327.
[36] M.F. Daniel, B. Desbat, J.C. Lassegues, B. Gerand, M. Figlarz, J. Solid State Chem. 67 (1987) 235–247.
[37] I.E. Wachs, F.D. Hardcastle, S.S. Chan, Spectroscopy (Eugene Oreg.) 1 (1986) 30.
[38] G.C. Bond, S. Flamerz, L.V. Wijk, Catal. Today 1 (1987) 229–243.
[39] D.C. Vermaire, P.C. Van Berge, J. Catal. 116 (1989) 309–317.
[40] K.S.W. Sing, D.H. Everett, R.A.W. Haul, L. Moscou, R.A. Pierotti, J. Rouquerol, T. Siemieniewska, Pure Appl. Chem. 57 (1985) 603–619.
[41] M. Luo, C. Wang, Y.S. Yan, Chem. Mater. 15 (2003) 3811–3814.
[42] H. Yamashita, Y. Ichihashi, S.G. Zhang, Y. Matrumura, Y. Souma, T. Tatsumi, M. Anpo, Appl. Surf. Sci. 121–122 (1997) 305–309.
[43] H. Tang, H. Berger, P.E. Schmid, F. Levy, G. Burri, Solid State Commun. 87 (1993) 847–850.
[44] H. Tang, K. Prasad, R. Sanjines, P.E. Schmid, F. Levy, J. Appl. Phys 75 (1994) 2042.
[45] M. Anpo, N. Alkawan, Y. Kubokaway, J. Phys. Chem. 23 (1985) 5017–5021.
[46] T. Toyoda, T. Hayakawa, K. Abe, T. Shigenari, Q. Shen, J. Lumin. 87–89 (2000) 1237.
[47] N. Bai, S.G. Li, H.Y. Chen, W.Q. Pang, J. Mater. Chem. 11 (2001) 3099.
[48] F.B. Li, X.Z. Li, Appl. Catal. A 228 (2002) 15.
[49] B.S. Liu, X.J. Zhao, L.P. Wen, Mater. Sci. Eng. B 134 (2006) 27.
[50] M. Srivasan, T. White, Environ. Sci. Technol. 41 (2007) 4405–4409.
[51] Y. Xin-Li, G. Ruihua, D. Wei-Lin, F. Kangnian, J. Phys. Chem. C 112 (2008) 3819–3826.
[52] A. Gulino, S. Parker, F.H. Jones, R.G. Egdell, J. Chem. Soc. Faraday Trans. 92 (12) (1996) 2137–2141.
[53] R. Andriy, S. Roland, O. Peter, B. Johannes, K. Ute, M. Daniel, S. Vladislav, J. Phys. Chem. C 112 (30) (2008) 11090–11092.
[54] G. Bifen, M. Ying, C. Yaan, Y. Wensheng, Y. Jiannian, J. Phys. Chem. B 110 (2006) 14391–14397.
[55] C. Martin, G. Solana, V. Rives, G. Marcı', L. Palmisano, A. Sclafani, Catal. Lett. 49 (1997) 235.
[56] G. Marci, L. Palmisano, A. Sclafani, A.M. Venezia, R. Campostrini, G. Carturan, C. Martin, V. Rives, G. Solana, J. Chem. Soc., Faraday Trans 92 (1996) 19.
[57] K. Tennakone, O.A. Heperuma, J.M.S. Bandara, W.C.B. Kiridena, Semicond. Sci. Technol. 7 (1992) 423.
[58] S.Y. Chai, Y.J. Kim, W.I. Lee, J. E. Electroceram. 17 (2006) 909–912.
[59] S.J. Wang, G. Cheng, X.H. Jiang, Y.C. Li, Y.B. Huang, Z.L. Du, Appl. Phys. Lett. 88 (2006) 212108.
[60] C.S. Fu, C. Lei, G. Shen, C.G. Yu, Powder Technol. 160 (2005) 198.
[61] D. Robert, Catal. Today 122 (2007) 20–26.
[62] V. Puddu, R. Mokaya, G.L. Chem, Communication 45 (2007) 4749–4756.
[63] J. Papp, S. Soled, K. Dwight, A. Wold, Chem. Mater. 6 (1994) 496–500.
[64] J.H. Pan, W.I. Lee, Chem. Mater. 18 (2006) 847.
[65] F.B. Li, G.B. Gu, X.J. Li, H.F. Wan, Acta Phys. -Chim. Sinica 16 (2000) 997–1002.
[66] K. Tanabe, T. Sumiyoshi, K. Shibata, T. Kiyoura, Kitagawa, J. Bull. Chem. Soc. Jpn. 47 (1974) 1061.
[67] T. Yamaguchi, Y. Tanaka, K. Tanabe, J. Catal. 65 (1980) 442.
[68] K. Shibata, T. Kiyoura, J. Kitagawa, T. Sumiyoshi, Tanabe, J. Bull. Chem. Soc. Jpn. 46 (1973) 2985.
[69] H. Tada, A. Kokubu, M. Iwasaki, S. Ito, Langmuir 20 (2004) 4665.
[70] A. Sobczynski, L. Duczmal, W. Zmudzinski, J. Mol. Catal. A: Chem. 213 (2004) 225–230.
[71] K.N. Agaveni, G. Sivalingam, M.S. Hegde, G. Madras, Environ. Sci. Technol. 38 (2004) 1600–1604.
[72] E. Leyva, E. Moctezuma, M.G. Ruiz, L.T. Martinez, Catal. Today 40 (1998) 367–376.
[73] M. Salaices, B. Serrano, H.I. De-Lasa, Chem. Eng. Sci. 59 (2004) 3–15.
[74] E.B. Azevedo, F.R.A. Neto, M. Dezotti, Appl. Catal. B 54 (2004) 165–173.
[75] V. Iliev, A. Mihaylova, L. Bilyarska, J. Mol. Catal. A 184 (2002) 121–130.
[76] V. Iliev, J. Photochem. Photobiol. A 151 (2002) 195–199.